Pre–mass extinction decline of latest Permian ammonoids

Wolfgang Kiessling[1], Martin Schobben[2,3], Abbas Ghaderi[4], Vachik Hairapetian[5], Lucyna Leda[2], and Dieter Korn[2]

[1]GeoZentrum Nordbayern, Department of Geography and Geosciences, Universität Erlangen–Nürnberg, Loewenichstraße 28, 91054 Erlangen, Germany
[2]Museum für Naturkunde, Leibniz Institute for Evolution and Biodiversity Science, Berlin, Invalidenstraße 43, 10115 Berlin, Germany
[3]School of Earth and Environment, University of Leeds, Woodhouse Lane, Leeds LS2 9JT, UK
[4]Department of Geology, Faculty of Science, Ferdowsi University of Mashhad, Azadi Square, 9177948974 Mashhad, Iran
[5]Department of Geology, Isfahan (Khorasgan) Branch, Islamic Azad University, PO Box 81595-158, Isfahan, Iran

ABSTRACT

The devastating end-Permian mass extinction is widely considered to have been caused by large-scale and rapid greenhouse gas release by Siberian magmatism. Although the proximate extinction mechanisms are disputed, there is widespread agreement that a major extinction pulse occurred immediately below the biostratigraphically defined Permian–Triassic boundary. Our statistical analyses of stratigraphic confidence intervals do not comply with a single end-Permian extinction pulse of ammonoids in Iran. High turnover rates and extinction pulses are observed over the last 700 k.y. of the Permian period in two widely separated sections representative of a larger area. Analyses of body sizes and morphological complexity support a gradual decline over the same interval. Similar pre–mass extinction declines and disturbances of the carbon cycle have sometimes been reported from other regions, suggesting a widespread, but often overlooked, environmental deterioration at a global scale, well before the traditional main extinction pulse.

INTRODUCTION

Patterns, ultimate causes, and consequences of the end-Permian mass extinction are increasingly well understood, but there is still controversy regarding the extinction mechanism (Baresel et al., 2017). Although the Siberian Traps are consistently being linked to the most profound mass extinction of the Phanerozoic (e.g., Brand et al., 2012; Burgess et al., 2017), the precise temporal match between volcanism and extinctions remains equivocal. On the paleontological side, there is an ongoing debate whether a single extinction pulse (Jin et al., 2000) or several extinction pulses (e.g., Xie et al., 2005; Song et al., 2013) are most likely. The main extinction pulse is universally recognized slightly below the biostratigraphically defined Permian-Triassic (P-Tr) boundary, and is currently dated at 251.94 Ma (Burgess et al., 2014). Authors arguing for two or more extinction pulses usually identify additional extinction pulses in younger strata. Gradual extinctions within the latest Permian (late Changhsingian) are sometimes suggested (Ward et al., 2005; Feng and Algeo, 2014; Wang et al., 2014) but not widely discussed in current extinction scenarios.

However, evidence is accumulating that environmental changes before the main extinction pulse were more substantial than previously thought (Korte and Kozur, 2010; Burgess and Bowring, 2015; Grasby et al., 2015), and thus pre–mass extinction dynamics should be revisited. The overwhelming majority of fossil data concerning the end-Permian mass extinction are from sections, where sequence-stratigraphic architecture may artificially concentrate last occurrences (Holland and Patzkowsky, 2015). To test our hypothesis of a gradual decline, we studied the succession of latest Permian ammonoids in two classical Iranian areas, where fossils are uniformly distributed in sections of monotonous deep-water limestones: the *Paratirolites* Limestone at Julfa in northwest Iran facing the Paleotethys, and Baghuk Mountain in central Iran facing the Neotethys (Fig. 1).
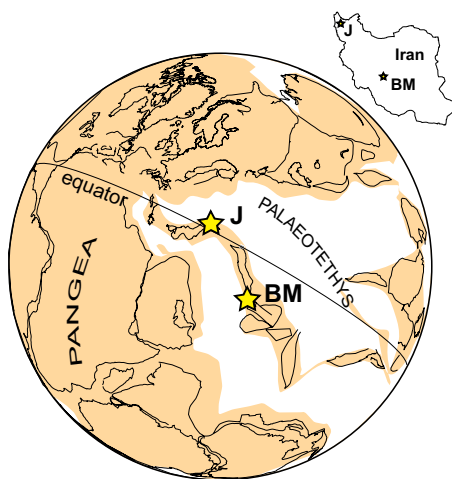

Figure 1. Present-day and late Permian location of the investigated Permian-Triassic boundary sections (Julfa [J], Iran: 38.94°N, 45.52°E; Baghuk Mountain [BM], Iran: 31.57°N, 52.44°E). Plate tectonic reconstruction is after Stampfli and Borel (2002).

MATERIALS AND METHODS

Geological Setting

The *Paratirolites* Limestone consists of a 4–5-m-thick, monotonous succession of red, marly, nodular limestone, rich in ammonoids (Korn et al., 2016). It is estimated to span 1.4 m.y., from 253.32 Ma to 251.94 Ma (Schobben et al., 2015), followed by a "boundary clay" without ammonoids (Leda et al., 2014) that ranges up to the formal P-Tr boundary (251.90 Ma). The microfacies is uniform in the *Paratirolites* Limestone except for an increasing amount of intraclasts and hardgrounds up section, suggesting reduced calcium carbonate accumulation rates approaching the P-Tr boundary (Leda et al., 2014).

Ammonoid Data

Nearly 600 ammonoid specimens, comprising 48 species, were collected in extensive field surveys. The sampling protocol for ammonoids was bulk-surface, without focusing on any particular stratigraphic interval within the *Paratirolites* Limestone. We tested statistically, if fossil recovery also complies with a random (uniform) distribution. After excluding species known from only a single stratigraphic horizon and making their last appearance below −4 m (see the Results section), we had available for analysis 21 species from 49 fossil horizons at Julfa, and 23 species from 54 horizons at Baghuk (Tables DR1 and DR2 in the GSA Data Repository[1]). Nine species occur in both sections.

Stratigraphic Ranges

We employed a variety of methods to assess the range of extinction scenarios that is consistent with the ammonoid record in Iran, but we focus here on simple older methods, focusing on the distribution of confidence intervals of local taxon ranges (Springer, 1990; Solow, 1996). Springer's method was repeated in a

---

loop, in which a pre-boundary clay extinction pulse is sought by successively moving down the section, while removing species reaching higher than the candidate boundary. With this approach, we iteratively estimate the possibility of extinction pulses prior to the deposition of the boundary clay. Solow's (1996) likelihood-ratio test was used to calculate an exact probability of recording ranges at least as extreme as those observed, assuming the null hypothesis of a common upper range endpoint were true.

Morphology

We gathered size measurements of 593 specimens of the ammonoid family Dzhulfitidae and computed the volume of the body chamber with a simple frustum volume equation, approximating unknown parameters from aperture shapes. Finally, we assessed morphological complexity by the number of notches on the external, adventive, and lateral lobes of the suture line (Korn, 2010). The overall temporal trend of both size and morphological complexity were assessed with local polynomial regression fitting, where the smoothing parameter was chosen with a bias-corrected Akaike's Information Criterion (AIC). All analyses were performed in R (R Core Team, 2015) and the fANCOVA package (Wang, 2010) was used for automated smoothing parameter selection.

RESULTS

A uniform distribution of fossil horizons is rejected for the entire thickness of the *Paratirolites* Limestone, but Kolmogorov-Smirnov (KS) tests and quantile-simulations *sensu* Solow et al. (2006) suggest a uniform distribution in the upper 4 m. We thus limit all analyses to the upper 4 m of the two sections, representing ~1.3 m.y. according to the age model of Schobben et al. (2015). Within this interval, all prerequisites are met for applying classical confidence interval methods (Wang and Marshall, 2016).

In spite of a large geographic distance between the two sections, patterns of last occurrences at Julfa and Baghuk are strikingly similar (Fig. 2). The observed ranges and their confidence intervals support a gradual or pulsed extinction prior to the deposition of the boundary clay, whereas the hypothesis of a simultaneous mass extinction in the boundary clay is rejected. Applying Solow's (1996) likelihood ratio statistic, the null hypothesis of a common endpoint of ammonoid species at the base of the boundary clay is strongly rejected ($p < 10^{-15}$) in both sections.

Potential extinction pulses are identified upon stepping down the *Paratirolites* Limestone in intervals of 10 cm, and repeatedly applying statistical tests for random range truncations complying with synchronous true range ends (Springer, 1990) (Fig. 2). At Julfa, local minima of D values of the KS test are found at 1.4 m and 2.5 m below the boundary clay. As a uniform
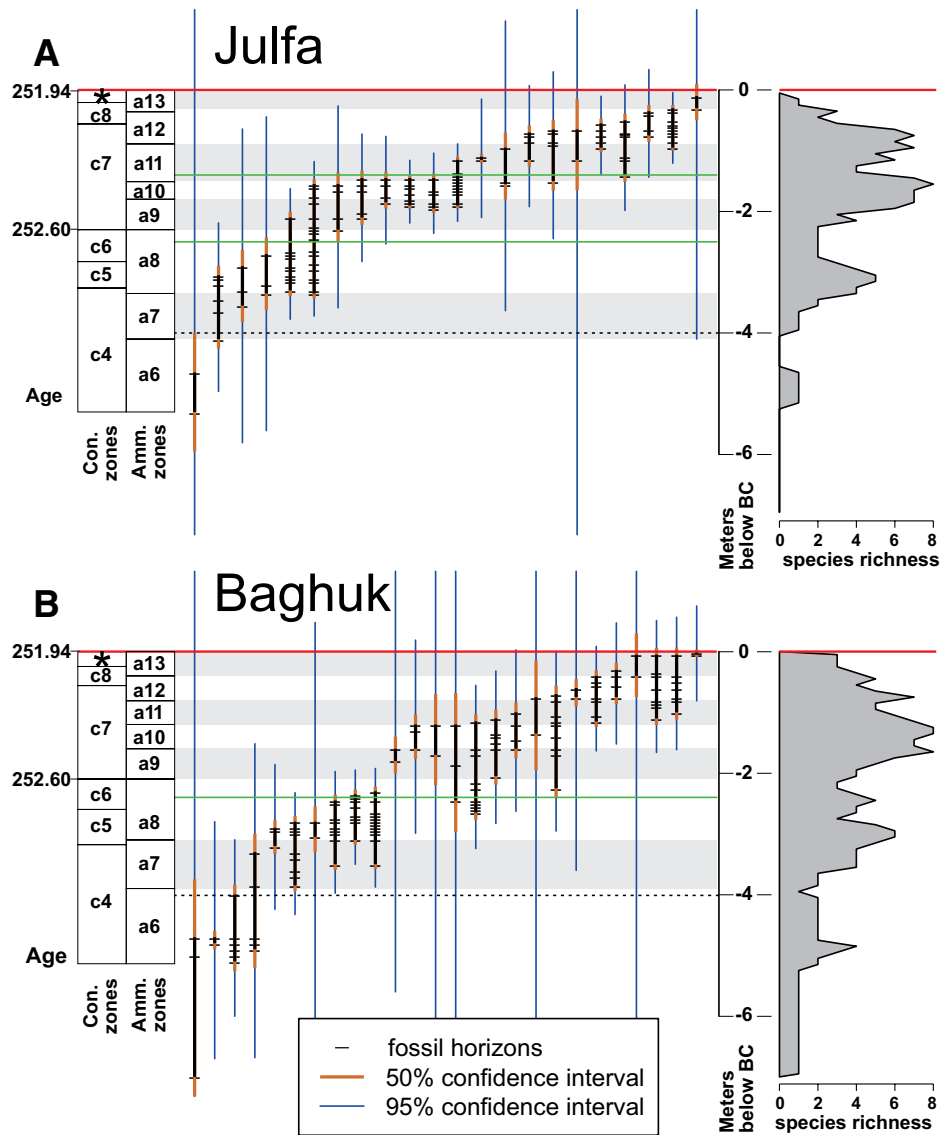

Figure 2. Stratigraphic ranges and species richness of late Changhsingian ammonites in Iran (A—Julfa; B—Baghuk Mountain). Singletons were omitted. Regional ammonite zones are shaded and labeled: a6—*Dzhulfites zalensis*; a7—*Paratirolites trapezoidalis;* a8—*Paratirolites kittli;* a9—*Stoyanowites dieneri;* a10—*Alibashites mojsisovicsi;* a11—*Abichites abichi;* a12—*Abichites stoyanowi;* a13—*Arasella minuta.* Corresponding conodont zones: c4—*Clarkina chanxingensis;* c5—*C. bachmanni;* c6—*C. nodosa;* c7—*C. yini;* c8—*C. abadehensis;* *(c9) —*C. hauschkei.* Absolute ages are based on Schobben et al. (2015). Confidence intervals of stratigraphic ranges were calculated based on Strauss and Sadler (1989). Occurrences below the black dashed line (at –4 m) were excluded from analyses. Thick red line marks the base of the boundary clay (BC) containing the main extinction pulse of benthic marine animals. Green lines indicate local minima of D values for which, moving down section, a uniform distribution of confidence intervals cannot be rejected (Kolmogorov-Smirnov test, following Springer, 1990). Species names and ranges are listed in Tables DR1 and DR2 (see footnote 1).

distribution of confidence intervals cannot be rejected for both these horizons ($p = 0.51$ and 0.78, respectively), they may represent extinction pulses. Two local D-value minima are also evident at Baghuk, at 0.9 m and 2.4 m below the boundary clay. However, the KS test fails to reject a uniform distribution of confidence intervals only for the 2.4 m horizon. In summary, two extinction pulses may exist at Julfa (1.4 and 2.5 m), whereas only one pulse is evident at Baghuk (2.4 m).

Although turnover rates are high throughout the *Paratirolites* Limestone (median species duration = 217 k.y.), these rates may just represent elevated background rates. Last appearances are indeed balanced by first appearances until the top meter of the *Paratirolites* Limestone, where standing diversity starts declining. Limiting analyses to this interval still rejects the null hypothesis of a common endpoint of species at the base of the boundary clay for Julfa ($p = 0.0002$) but not for Baghuk ($p = 0.23$).

The lowest level at which the hypothesis of a common endpoint at the boundary clay is not rejected is 0.5 m at Julfa (for three species) and 1.3 m at Baghuk (for 10 species).

There is a pronounced trend toward smaller body size of ammonoids in both study areas, but the trend is not monotonic (Fig. 3). The decrease of average body size is largely manifested in the successive extirpation of larger taxa and the appearance of smaller taxa. The top levels of the *Paratirolites* Limestone are dominated by minute forms such as *Arasella minuta*, *Abichites terminalis*, and *Abichites shahriari*. A similar trend is displayed in morphological complexity. There is a significant reduction in the number of notches in the external, adventive, and lateral lobes toward the boundary clay (Fig. 4). Although body size and sutural complexity are significantly cross-correlated (R = 0.49 for Julfa and R = 0.44 for Baghuk, based on first differences), the unexplained variance suggests that morphological simplification is not entirely tied to body size.

DISCUSSION

A single ammonoid extinction pulse at the base of the Iranian boundary clay is strongly rejected for the top 4 m of the *Paratirolites* Limestone. This interval records one (Baghuk) or two (Julfa) extinction pulses, and otherwise high turnover rates. In spite of the distinct facies change from the *Paratirolites* Limestone into the boundary clay, there is no hint of an extinction pulse at this boundary at Julfa, except for the last three species in the top 0.5 m. The situation is different at Baghuk, where the hypothesis of a simultaneous extinction is not rejected for 10 species occurring in top 1.3 m. However, facies change rather than a true extinction pulse may explain the range truncations, similar to many other sections.

A pre-boundary extinction pulse in the regional *Paratirolites kittli* ammonoid zone is recognized in both study areas. This is the same biozone in which body size and morphological complexity started declining. This biozone is correlated with the *Clarkina nodosa* conodont zone (lower *C. yini* zone in South China), thought to be centered at ca. 252.6 Ma (Schobben et al., 2015); that is, ~700 k.y. before the main extinction pulse in China. This is also the time of onset of a long-term negative carbonate $\delta^{13}C$ excursion at a global scale (Korte and Kozur, 2010; Schobben et al., 2017).

The concordance of morphological simplification, decreasing body size, and extinction may indicate a common cause. Both the decrease of sutural complexity and the decrease of body size can be explained by heterochrony, the change in the timing of ontogenetic events. The adult specimens approaching the P-Tr boundary appear like juveniles in older parts of the sections, suggesting pedomorphosis, which may be linked to environmental instability (McKinney, 1986).

Figure 3. Decline of late Changhsingian ammonoid (Dzhulfitidae) sizes in Iran. Size is approximated by the volume of the body chamber. Red lines represent local polynomial regression fitting (LOESS, LOcal polynomial regrESSion fitting) with an Akaike's Information Criterion (AIC)-selected optimal smoothing parameter (0.41 for Julfa, 0.21 for Baghuk). Ammonite zones are shaded as in Figure 2. The dominant, identified genera are colored: purple—*Paratirolites*; brown—*Alibashites*, orange—*Abichites*, green—*Stoyanowites*.
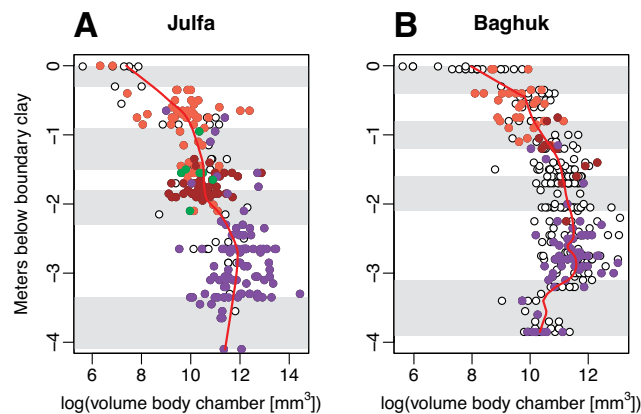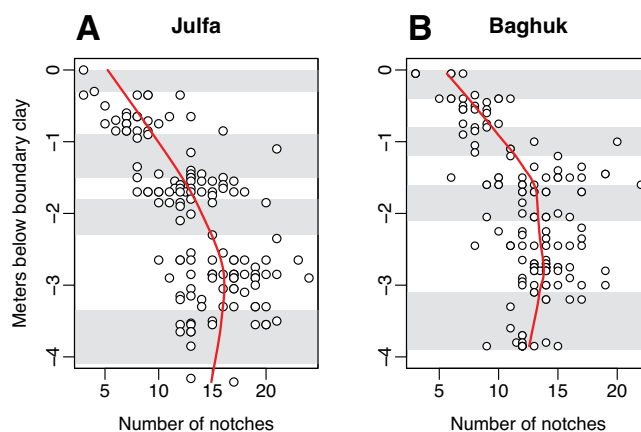

Figure 4. Decline of morphological complexity assessed by the number of notches of ammonoid suture lines. LOESS smoothing as in Figure 3 (parameters are 0.74 for Julfa and 0.63 for Baghuk, Iran) and shading of ammonite zones as in Figure 2.

Although strictly applicable only to Iranian ammonoids, our study adds to the growing body of evidence that environmental stress was above background in the last million years of the Permian period, and that this stress affected organisms more than commonly assumed. For example, a late Changhsingian decline of body size has been noted in brachiopods of South China (He et al., 2007; Zhang et al., 2016), which in Guizhou is also associated with community turnover (Zhang et al., 2017). A substantial pre–mass extinction decline was also noted for radiolarians in deep-water sections (Feng et al., 2007; Feng and Algeo, 2014). The first of three fly ash events in Arctic Canada, attributed to Siberian coal burning, is dated to 500–750 k.y. before the main extinction pulse and also marked by the onset of a gradual, negative $\delta^{13}C$ excursion (Grasby et al., 2011).

We conclude that the end-Permian mass extinction had a prelude leading to extinction pulses, and a substantial decline of body size and morphological simplification in latest Permian ammonoids. Radiolarians, and perhaps brachiopods, were also affected but there are no reliable records for other marine invertebrates. A geologically brief extinction episode at the Permian-Triassic boundary (Burgess et al., 2014) appears unlikely given the pre-extinction history (this study) and the sequence-stratigraphically controlled range truncations in most shallow-water sections (Holland and Patzkowsky, 2015).

REFERENCES CITED
Baresel, B., Bucher, H., Bagherpour, B., Brosse, M., Guodun, K., and Schaltegger, U., 2017, Timing of global regression and microbial bloom linked with the Permian-Triassic boundary mass extinction: implications for driving mechanisms: Scientific Reports, v. 7, p. 43630, https://doi.org/10.1038/srep43630.
Brand, U., Posenato, R., Came, R., Affek, H., Angiolini, L., Azmy, K., and Farabegoli, E., 2012, The end-Permian mass extinction: A rapid volcanic CO_2 and CH_4-climatic catastrophe: Chemical

Geology, v. 322–323, p. 121–144, https://doi.org /10.1016/j.chemgeo.2012.06.015.

Burgess, S.D., Bowring, S., and Shen, S.-z., 2014, High-precision timeline for Earth's most severe extinction: Proceedings of the National Academy of Sciences of the United States of America, v. 111, p. 3316–3321, https://doi.org/10.1073/pnas .1317692111 (erratum available at https://doi.org /10.1073/pnas.1403228111).

Burgess, S.D., and Bowring, S.A., 2015, High-precision geochronology confirms voluminous magmatism before, during, and after Earth's most severe extinction: Science Advances, v. 1, p. e1500470, https://doi.org/10.1126/sciadv.1500470.

Burgess, S.D., Muirhead, J.D., and Bowring, S.A., 2017, Initial pulse of Siberian Traps sills as the trigger of the end-Permian mass extinction: Nature Communications, v. 8, p. 164, https://doi.org /10.1038/s41467-017-00083-9.

Feng, Q., and Algeo, T.J., 2014, Evolution of oceanic redox conditions during the Permo-Triassic transition: Evidence from deepwater radiolarian facies: Earth-Science Reviews, v. 137, p. 34–51, https://doi.org/10.1016/j.earscirev.2013.12.003.

Feng, Q., He, W., Gu, S., Meng, Y., Jin, Y., and Zhang, F., 2007, Radiolarian evolution during the latest Permian in South China: Global and Planetary Change, v. 55, p. 177–192, https://doi.org /10.1016/j.gloplacha.2006.06.012.

Grasby, S.E., Beauchamp, B., Bond, D.P.G., Wignall, P., Talavera, C., Galloway, J.M., Piepjohn, K., Reinhardt, L., and Blomeier, D., 2015, Progressive environmental deterioration in northwestern Pangea leading to the latest Permian extinction: Geological Society of America Bulletin, v. 127, p. 1331–1347, https://doi.org/10.1130/B31197.1.

Grasby, S.E., Sanei, H., and Beauchamp, B., 2011, Catastrophic dispersion of coal fly ash into oceans during the latest Permian extinction: Nature Geoscience, v. 4, p. 104–107, https://doi.org /10.1038/ngeo1069.

He, W., Shi, G.R., Feng, Q., Campi, M.J., Gu, S., Bu, J., Peng, Y., and Meng, Y., 2007, Brachiopod miniaturization and its possible causes during the Permian-Triassic crisis in deep water environments, South China: Palaeogeography, Palaeoclimatology, Palaeoecology, v. 252, p. 145–163, https://doi.org/10.1016/j.palaeo.2006.11.040.

Holland, S.M., and Patzkowsky, M.E., 2015, The stratigraphy of mass extinction: Palaeontology, v. 58, p. 903–924, https://doi.org/10.1111/pala.12188.

Jin, Y.G., Wang, Y., Wang, W., Shang, Q.H., Cao, C.Q., and Erwin, D.H., 2000, Pattern of marine mass extinction near the Permian-Triassic boundary in South China: Science, v. 289, p. 432–436, https:// doi.org/10.1126/science.289.5478.432.

Korn, D., 2010, A key for the description of Palaeozoic ammonoids: Fossil Record (Weinheim), v. 13, p. 5–12, https://doi.org/10.1002/mmng.200900008.

Korn, D., Ghaderi, A., Leda, L., Schobben, M., and Ashouri, A.R., 2016, The ammonoids from the Late Permian *Paratirolites* Limestone of Julfa (East Azerbaijan, Iran): Journal of Systematic Palaeontology, v. 14, p. 841–890, https://doi.org /10.1080/14772019.2015.1119211.

Korte, C., and Kozur, H.W., 2010, Carbon-isotope stratigraphy across the Permian–Triassic boundary: A review: Journal of Asian Earth Sciences, v. 39, p. 215–235, https://doi.org/10.1016/j.jseaes .2010.01.005.

Leda, L., Korn, D., Ghaderi, A., Hairapetian, V., Struck, U., and Reimold, W.U., 2014, Lithostratigraphy and carbonate microfacies across the Permian–Triassic boundary near Julfa (NW Iran) and in the Baghuk Mountains (Central Iran): Facies, v. 60, p. 295–325, https://doi.org/10.1007/s10347-013 -0366-0.

McKinney, M.L., 1986, Ecological causation of heterochrony: A test and implications for evolutionary theory: Paleobiology, v. 12, p. 282–289, https:// doi.org/10.1017/S0094837300013786.

R Core Team, 2015, A language and environment for statistical computing: R Foundation for Statistical Computing: Vienna, Austria, https://www.R-project.org/.

Schobben, M., Stebbins, A., Ghaderi, A., Strauss, H., Korn, D., and Korte, C., 2015, Flourishing ocean drives the end-Permian marine mass extinction: Proceedings of the National Academy of Sciences of the United States of America, v. 112, p. 10298–10303, https://doi.org/10.1073/pnas .1503755112.

Schobben, M., et al., 2017, Latest Permian carbonate-carbon isotope variability traces heterogeneous organic carbon accumulation and authigenic carbonate formation: Climate of the Past, v. 13, p. 1635–1659, https://doi.org/10.5194/cp-13 -1635-2017.

Solow, A.R., 1996, Tests and confidence intervals for a common upper endpoint in fossil taxa: Paleobiology, v. 22, p. 406–410, https://doi.org/10.1017 /S0094837300016353.

Solow, A.R., Roberts, D.L., and Robbirt, K.M., 2006, On the Pleistocene extinctions of Alaskan mammoths and horses: Proceedings of the National Academy of Sciences of the United States of America, v. 103, p. 7351–7353, https://doi.org /10.1073/pnas.0509480103.

Song, H., Wignall, P.B., Tong, J., and Yin, H., 2013, Two pulses of extinction during the Permian-Triassic crisis: Nature Geoscience, v. 6, p. 52–56, https://doi.org/10.1038/ngeo1649.

Springer, M.S., 1990, The effect of random range truncations on patterns of evolution in the fossil record: Paleobiology, v. 16, p. 512–520, https:// doi.org/10.1017/S0094837300010228.

Stampfli, G.M., and Borel, G.D., 2002, A plate tectonic model for the Paleozoic and Mesozoic constrained by dynamic plate boundaries and restored synthetic oceanic isochrons: Earth and Planetary Science Letters, v. 196, p. 17–33, https:// doi.org/10.1016/S0012-821X(01)00588-X.

Strauss, D., and Sadler, P.M., 1989, Classical confidence intervals and Bayesian probability estimates for ends of local taxon ranges: Mathematical Geology, v. 21, p. 411–427, https://doi.org/10 .1007/BF00897326.

Wang, S.C., and Marshall, C.R., 2016, Estimating times of extinction in the fossil record: Biology Letters, v. 12, p. 20150989, https://doi.org/10 .1098/rsbl.2015.0989.

Wang, X.-F., 2010, fANCOVA: Nonparametric Analysis of Covariance: R package version 0.5–1: The Comprehensive R Archive Network, https:// cran.r-project.org/web/packages/fANCOVA /fANCOVA.pdf.

Wang, Y., Sadler, P.M., Shen, S.-z., Erwin, D.H., Zhang, Y.-c., Wang, X.-d., Wang, W., Crowley, J.L., and Henderson, C.M., 2014, Quantifying the process and abruptness of the end-Permian mass extinction: Paleobiology, v. 40, p. 113–129, https://doi.org/10.1666/13022.

Ward, P.D., Botha, J., Buick, R., De Kock, M.O., Erwin, D.H., Garrison, G.H., Kirschvink, J.L., and Smith, R., 2005, Abrupt and gradual extinction among Late Permian land vertebrates in the Karoo Basin, South Africa: Science, v. 307, p. 709– 714, https://doi.org/10.1126/science.1107068.

Xie, S., Pancost, R.D., Yin, H., Wang, H., and Evershed, R.P., 2005, Two episodes of microbial change coupled with Permo/Triassic faunal mass extinction: Nature, v. 434, p. 494–497, https://doi .org/10.1038/nature03396.

Zhang, Y., Shi, G.R., He, W.-h., Wu, H.-t., Lei, Y., Zhang, K.-x., Du, C.-c., Yang, T.-l., Yue, M.-l., and Xiao, Y.-f., 2016, Significant pre-mass extinction animal body-size changes: Evidences from the Permian–Triassic brachiopod faunas of South China: Palaeogeography, Palaeoclimatology, Palaeoecology, v. 448, p. 85–95, https://doi.org/10.1016/j.palaeo.2015.11.020.

Zhang, Y., Shi, G.R., Wu, H.-t., Yang, T.-l., He, W.-h., Yuan, A.-h., and Lei, Y., 2017, Community replacement, ecological shift and early warning signals prior to the end-Permian mass extinction: A case study from a nearshore clastic-shelf section in South China: Palaeogeography, Palaeoclimatology, Palaeoecology, v. 487, p. 118–135, https://doi.org/10.1016/j.palaeo.2017.07.042.